QUANTIFYING THE SIZE DISTRIBUTION OF RIVERS ACROSS SPATIAL SCALES

C.A. Boyd[1] and G.H. Allen[1]

[1]Department of Geosciences, Virginia Tech, Blacksburg, VA

Abstract

The surfaces of rivers are hotspots for biogeochemical exchange and emit significant amounts of greenhouse gases globally. Estimates of river surface area are critical to determining fluvial greenhouse gas evasion yet are currently poorly constrained. The relative abundance of narrow rivers to wide rivers is commonly assumed to be fractal, or scale invariant. This assumption aids in statistical estimates of river surface area but has not been tested across spatial scales. We measure river size in four nested basins within the Mississippi River Basin using a combination of remote sensing and field surveying to determine the statistical size distribution of rivers from continental to headwater scales. We find that the relative abundance of narrow rivers to wide rivers consistently fits a log-normal probability density function, supporting the assumption of fractal river size. Using the fractal size distribution of rivers, we estimate a total river surface area of 17,828 km^2 (0.54% of land surface area) in the Mississippi River Basin which is comparable to previous studies. Our multi-scale approach reveals the fractal nature of river size and allows for a more accurate accounting of river surface area with implications for the role of rivers in biogeochemical cycling.

1. Introduction

The surfaces of rivers and streams are an interface for biogeochemical exchange between Earth's inland waters and atmosphere. For example, rivers and streams (hereafter referred to collectively as rivers) emit about 20% of the carbon dioxide (CO_2) (Raymond et al., 2013), 17% of the methane (CH_4) (Rosentreter et al., 2021), and 1% of the nitrous oxide (N_2O) (Ciais et al., 2014; Marzadri et al., 2021) that are emitted from anthropogenic sources. Because of their importance in global biogeochemical cycles, greenhouse gas emissions from rivers are included in global carbon budget evaluations (Lauerwald et al., 2023). Fluvial-atmosphere gas exchange is typically modeled as a function of river surface area, gas transfer velocity, and the gas concentration gradient between water and the atmosphere (Liss & Slater, 1974; Richey et al., 2002). Therefore, accurate estimation of global river surface area is critical to determining the magnitude of fluvial greenhouse gas flux to the atmosphere.

However, global estimates of river surface area vary widely between studies. Recent estimates range from 363,000 km^2 (0.24% of land surface area) (Linke et al., 2019) to 811,000 km^2 (0.54% of land surface area) (Liu et al., 2022), and there are uncertainties in the relative abundance of narrow rivers to wide rivers. It is not feasible to hand survey global river surface area because rivers are spatially distributed on the landscape and river extent is dynamic through space and time. Additionally, rivers are often completely or partially obscured by overhanging vegetation in optical remote sensing imagery. These gaps in our understanding and limitations in observational capabilities introduce significant uncertainty in accounting for the role of rivers in global biogeochemical cycling.

In particular, small rivers are poorly accounted for in current estimates of river surface area. Their large number makes them difficult to inventory at a global scale and their small size makes them difficult to detect from remote sensing data. For example, the National Hydrography Dataset, a vector dataset representing the mapped locations of surface water in the United States published by the United States Geological Survey, has been shown to underestimate drainage density in headwater catchments by a factor of 3 (Benstead & Leigh, 2012; Meyer & Wallace, 2001). However, the surfaces of small rivers are particularly important to account for because they are more profuse emitters due to their higher slope, higher turbidity, low flow depth, and higher organic matter content (Hotchkiss et al., 2015; Marzadri et al., 2021).

Previous studies that estimate river surface area at a global scale make an assumption of scale invariance. The paradigm in fluvial geomorphology is to view river networks as fractals (Mandelbrot & Wheeler, 1983; Tarboton et al., 1988; La Barbera & Rosso, 1989; Nikora, 1991; Nikora & Sapozhnikov, 1993; Nikora, 1994; Rodriguez-Iturbe & Rinaldo, 1997; Martinez et al., 2022), where the statistical characteristics of river size are similar across spatial scales. Many studies estimate river geometry via at-a-station and downstream hydraulic geometry frameworks (Leopold & Maddock, 1953) which utilize the same scaling coefficients for rivers of all sizes (Raymond et al., 2013; Linke et al., 2019; Liu et al., 2022; Andreadis et al., 2013). However, previous work shows that this approach is analytically invalid because these river width scaling coefficients are scale dependent (Dingman, 2007; Grison et al., 2021). Allen and Pavelsky use the size distribution of rivers, or the statistical distribution of regularly spaced river width measurements, to make a statistical estimate of global surface area. They found that rivers wider than 90 m have a size distribution that is best represented by a Pareto (or power law) function and extrapolated this function to estimate the surface area of smaller rivers (Allen & Pavelsky, 2018). This approach also assumes that the size distribution of rivers does not change as river size decreases.

Recent work indicates that the size distribution of river surface area may not be consistent across spatial scales. The size distribution of large rivers (widths ≥ 90 m) has been described by a Pareto function (Allen & Pavelsky, 2018); however, field surveys of river width and length in headwater catchments (widths ≤ 5 m) reveal size distributions that are consistently described by a log-normal function, regardless of hydrologic or geomorphic context (Allen et al., 2018). The size distribution of medium sized rivers (between 5 m and 90 m wide) has not been described. This illustrates a gap in our understanding of the distribution of rivers of different sizes on the landscape with implications for riparian ecological functions that scale with river size (McIntosh et al., 2024), statistical estimates of global river surface area, and therefore, the role of rivers in global greenhouse gas emissions.

The goal of this study is to describe the statistical distribution of river width across spatial scales to determine if the assumption of scale invariance is appropriate for using statistical methods to estimate river surface area. We use a nested basin approach to measure river widths at four spatial scales and resolutions within the Mississippi River Basin. We also use the statistical distributions of widths by Strahler stream order (Strahler, 1952; Strahler, 1957) to estimate total river surface area in the Mississippi River Basin.

2. Methods

To investigate the size distribution of rivers at different spatial scales, we measured river widths using a combination of optical remote sensing imagery and fieldwork in four nested basins (see Fig. 1). At the largest spatial scale, the Mississippi River Basin, we used Landsat multispectral satellite imagery (30 m spatial resolution) derived river width measurements from the Global River Widths from Landsat (GRWL) database (Allen & Pavelsky, 2018). In the Platte River Basin, we used a mosaic of the least cloudy Sentinel-2 multispectral satellite imagery (10 m spatial resolution) from July-August 2019 to measure river width. In the St. Vrain Creek Basin, we used a mosaic of National Agriculture Imagery Program (NAIP) four band aerial imagery (1 m spatial resolution) from July-August 2021 to measure river width. In the South St. Vrain Creek Basin, we measured river widths by hand in the field between July 6 – August 6, 2023. Study areas were chosen for their size, ability to be viewed from above with minimal obscuring vegetation, and convenience for fieldwork. Image dates and fieldwork timing were chosen to match the seasonal availability of NAIP imagery (July-August).

Using remote sensing data from the Google Earth Engine catalogue, we created water masks (see Fig. 2) from images using the Normalized Difference Water Index (NDWI) (McFeeters, 1996):

$$NDWI = \frac{Green - NIR}{Green + NIR} \quad (1)$$

and the near infrared (NIR) band. Scene specific thresholds were chosen for both NDWI and NIR using the Otsu image segmentation technique to maximize the variance between “water” and “not

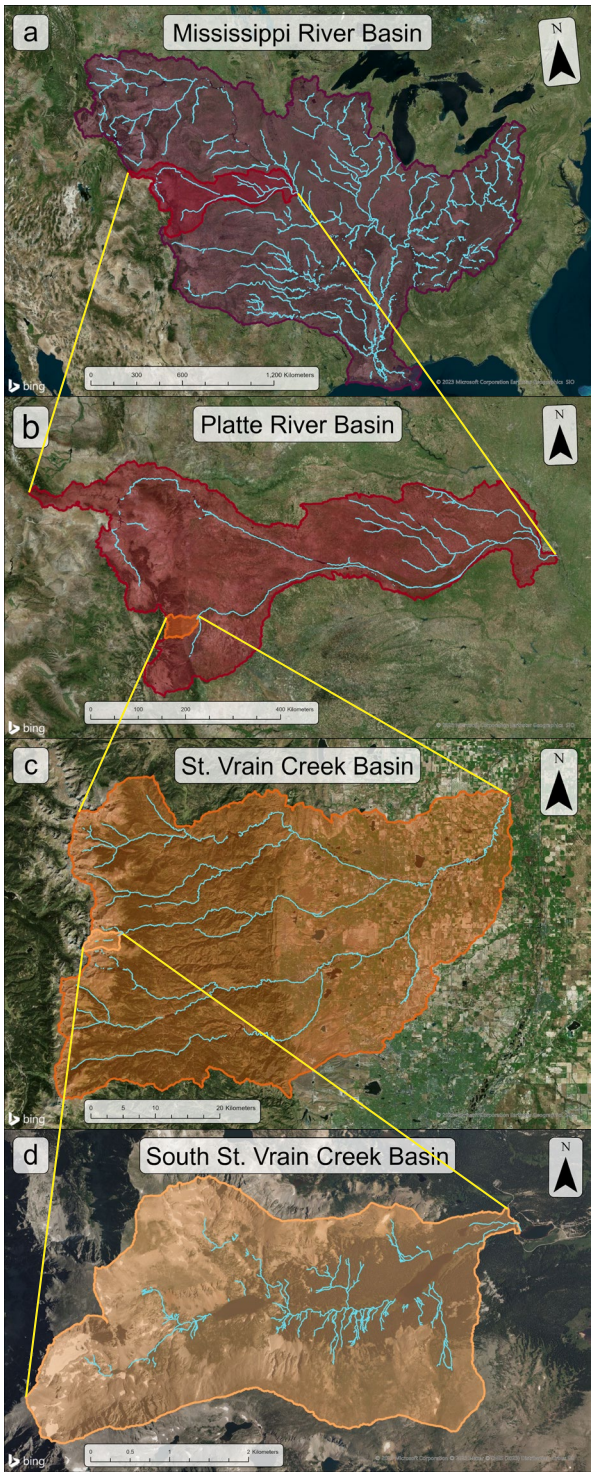

Figure 1. Maps showing study areas and measured rivers. a) Mississippi River Basin and river centerlines from GRWL. b) Platte River Basin and rivers measured with Sentinel-2. c) St. Vrain Creek Basin and rivers measured with NAIP. d) South St. Vrain Creek Basin and rivers measured by hand in the field.

water" classes (Otsu, 1979). From the water masks, we isolated the river network, and measured river width orthogonal to river centerlines using a modified version of the RivSelect and RivWidth routines in ENVI+IDL (Pavelsky & Smith, 2008). River width measurements from remote sensing were validated using a linear regression to USGS reported widths at co-located gaging stations within 10% of mean annual discharge in each basin. In the field, we paced the entire river network in the South St. Vrain Creek Basin and measured the width of water flowing in channels every 10 m.

We classified all river widths using Strahler stream order, a common method of describing river morphology, to make our analysis comparable with other studies. We manually assigned stream order to river widths measured in the field and spatially joined stream order from NHDPlus V2 to river widths measured using remote sensing. It has been widely reported that large scale hydrographic datasets underestimate stream order in headwater catchments (Benstead & Leigh, 2012; Fritz et al., 2013; Raymond et al., 2013); we found a discrepancy of three stream orders between NHDPlus V2 and the rivers we surveyed in the field. To account for this discrepancy, we increased stream order for remotely sensed river widths by three to match field observations.

To estimate the total river surface area in the Mississippi River Basin, we used the statistical distribution of measured river widths of each stream order and the total length of rivers of each order to generate regularly spaced synthetic river widths for the entire Mississippi River Basin. To determine the size distribution for each stream order, we fit log-normal (Eq. 2), Pareto (Eq. 3), gamma (Eq. 4), and Weibull (Eq. 5) probability density functions to our river width data:

$$f(x) = \frac{e^{-\frac{(\ln(x)-\mu)^2}{2\sigma^2}}}{x\sigma\sqrt{2\pi}} \quad (2)$$

$$f(x) = \frac{\alpha x_m^{\alpha}}{x^{\alpha+1}} \quad (3)$$

$$f(x) = \frac{x^{\alpha-1}e^{-\beta x}\beta^{\alpha}}{(\alpha-1)!} \text{ for } x,\alpha,\beta > 0 \quad (4)$$

$$f(x) = \frac{\gamma}{\alpha}\left(\frac{x}{\alpha}\right)^{(\gamma-1)}e^{-\left(\frac{x}{\alpha}\right)^{\gamma}} \text{ for } \gamma,\alpha > 0 \quad (5)$$

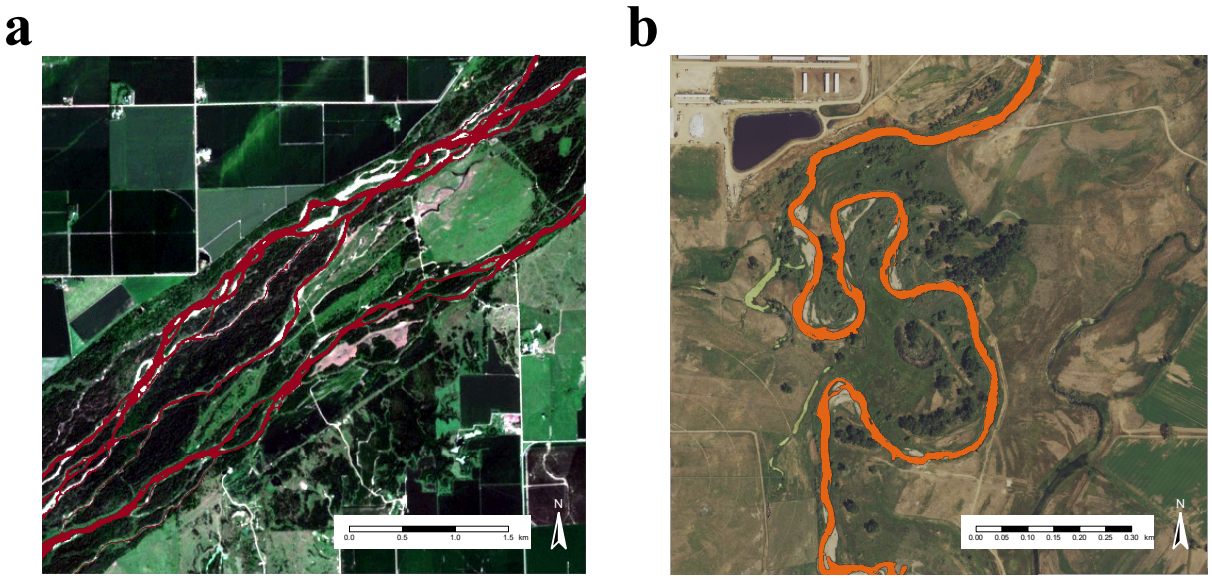

Figure 2. a) Water mask (red) from Sentinel-2 multispectral satellite imagery with a true color basemap; b) Water mask (orange) from NAIP four band aerial imagery with a true color basemap.

We sampled all width data to a uniform length interval of 30 m and used maximum likelihood estimation to determine the parameters of each distribution fitted to width measurements of each stream order. We assessed the goodness of fit for each distribution with a single sample, two-tailed Kolmogorov-Smirnov test (Venables & Ripley, 2002) (see Table S2). We estimated the total length of rivers of each order using Horton scaling principles which relate stream order to the number of rivers and average length of rivers in a basin (Horton, 1945; Downing et al., 2012) (see Fig. S1 and Table S3). We then used the best fit distribution, the measurement spacing interval, and the total length of rivers of each order to generate regularly spaced (30 m) synthetic widths for rivers of each stream order in the Mississippi River Basin. We multiplied each synthetic river width by the length spacing interval and summed to estimate total river surface area in the Mississippi River Basin.

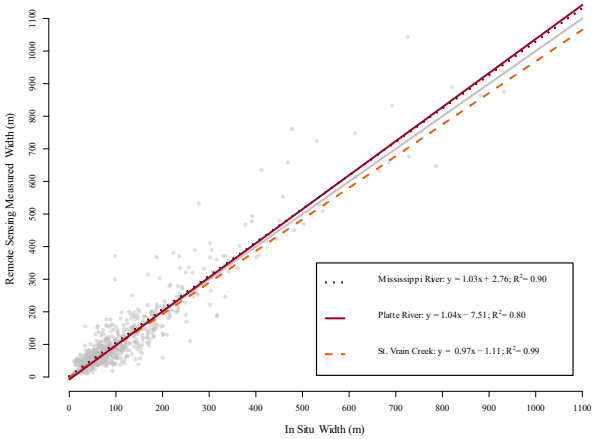

Figure 3. Validation of remote sensing measured river widths plotted against in-situ measured widths at USGS gaging stations. Linear regressions calculated using Sen's slope. Grey points represent co-located in-situ and remote sensing measured river widths. The grey line shows a 1:1 slope.

3. Results

River widths measured from remote sensing show good agreement with in-situ measured widths reported at USGS gaging stations (see Fig. 3). Linear regressions between remote sensing measured widths and in-situ reported widths show slopes close to 1 (1.03 and 1.04) and high R^2 (0.90 and 0.80) for the Mississippi River Basin and Platte River Basin measurements, respectively. The availability of NAIP imagery during the leaf-on period does not correspond to the time of year when rivers in the St. Vrain Creek Basin are typically at mean annual discharge. Therefore, we corrected NAIP measured widths using a regional rating curve (see Supplemental Methods), improving the linear regression slope between remote sensing measured widths and in-situ reported widths from 0.78 to 0.97 in the St. Vrain Creek Basin with an $R^2 = 0.99$.

Using maximum likelihood estimation to fit known statistical distributions to river width measurements by stream order, we find that the width distribution of rivers of each order are best described by a log-normal function on average (see Fig. 4). Using the length ratio (2.2) and bifurcation ratio (4.0) (see Fig. S1) in the Mississippi River Basin from NHDPlus V2, we find that the total length of rivers in the Mississippi River Basin is 4,823,609 km^2 (see Table S3). Using the size distribution of measured rivers of each stream order and estimates of total river length of each stream order from Horton scaling principles (Horton, 1945) (see Fig. S1) to generate a synthetic width dataset covering the entire Mississippi River Basin, we estimate that the total river surface area in the Mississippi River Basin is 17,828 km^2, or 0.54% of land surface area.

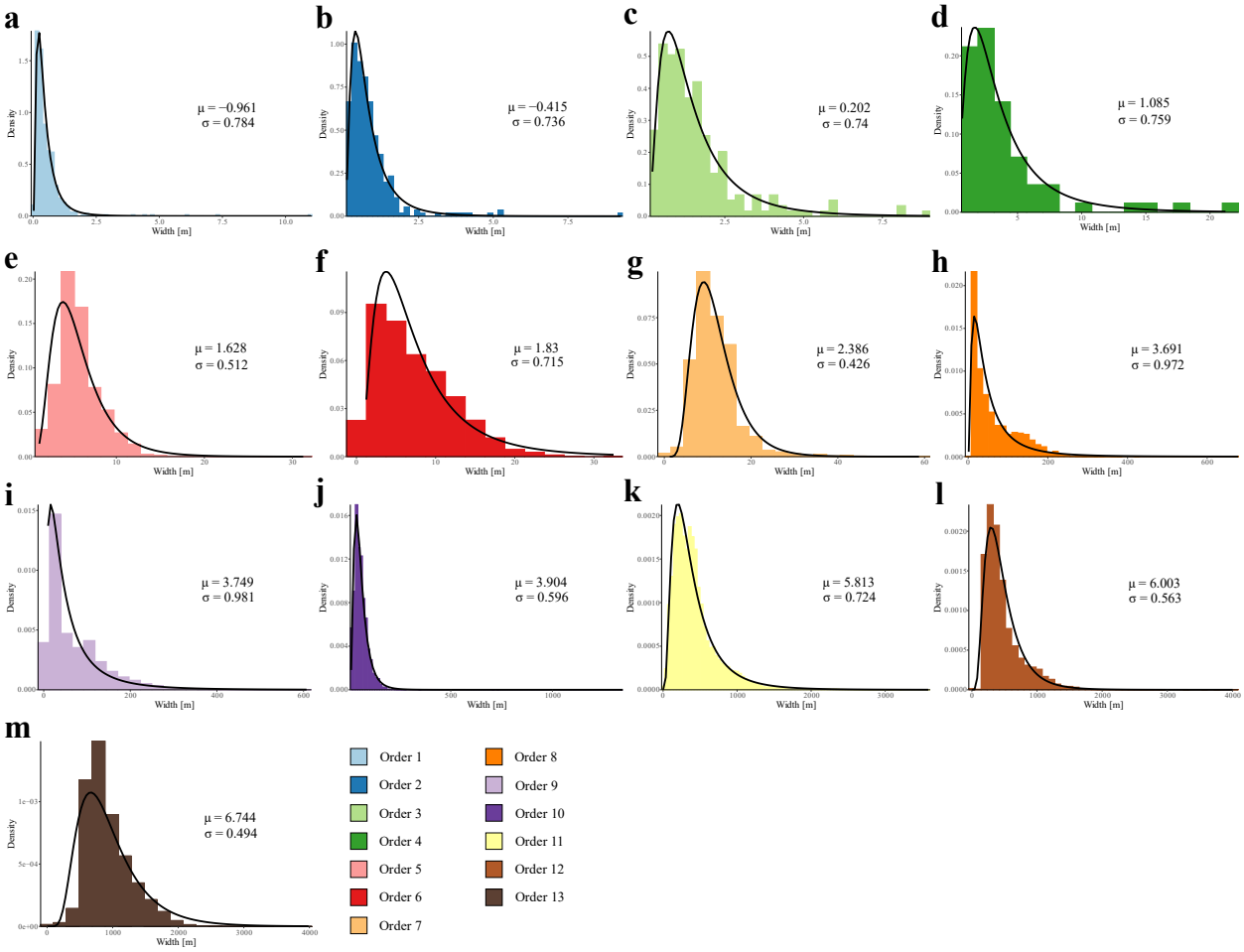

Figure 4. Density plots of measured river widths by stream order with fitted log-normal functions.

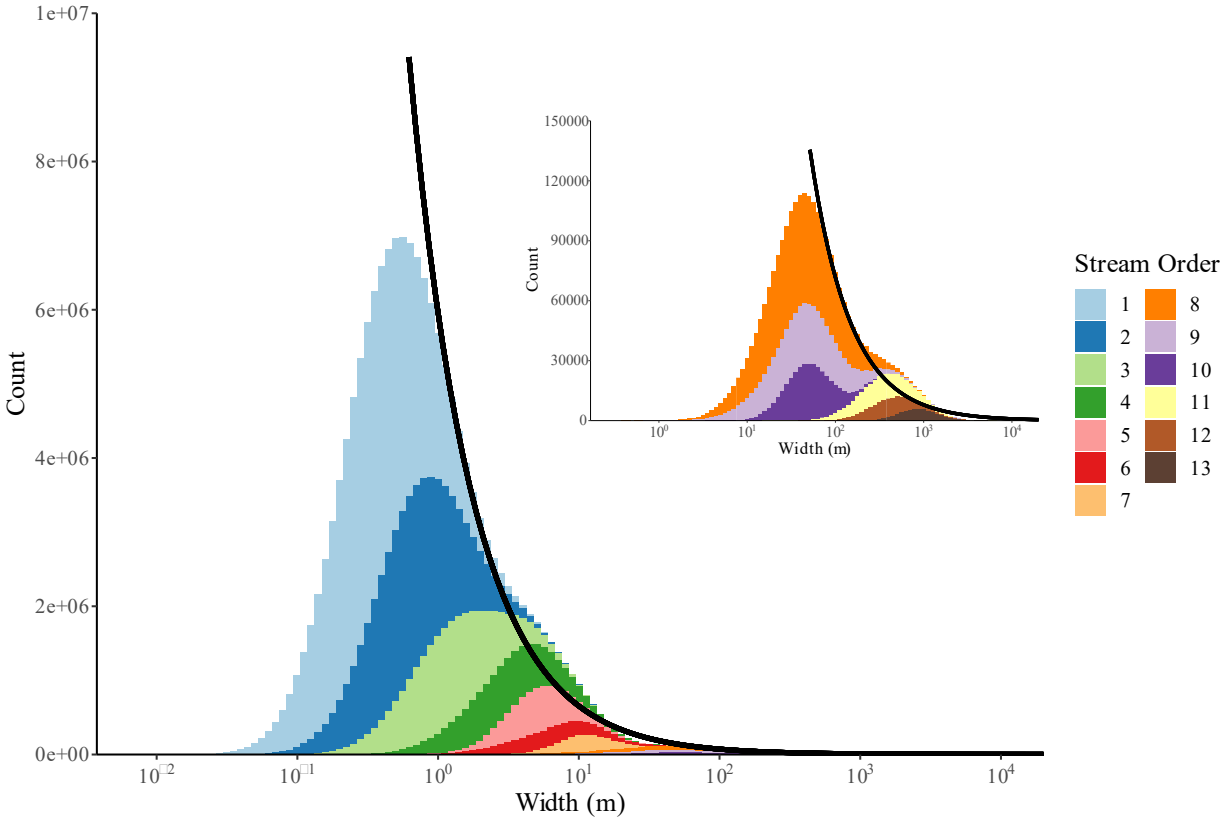

Figure 5. Stacked histogram of synthetic river widths covering the Mississippi River Basin, colored by stream order. The Pareto size distribution (Allen & Pavelsky, 2018) for rivers in the Mississippi River Basin is shown in black for comparison. Inset graph shows stream orders 8-13.

4. Discussion

There is both theoretical (Kirchner, 1993; Rodriguez-Iturbe & Rinaldo, 1997) and empirical (Leopold & Maddock, 1953; Rodriguez-Iturbe & Rinaldo, 1997) evidence supporting the fractal nature of river networks across a large range of spatial scales. Rodriguez-Iturbe and Rinaldo posit that the process of network formation in nature (like river basins) occurs in a way that minimizes the total energy expenditure of those networks both locally and in the network as a whole. Using the concept of Optimal Channel Networks (OCNs), they show that self-similar fractal river networks arise because of the need for effective connectivity and transmittance of flow (Rodriguez-Iturbe & Rinaldo, 1997). However, these analyses demonstrate the fractal *structure of river networks* and do not explicitly demonstrate the fractal nature of *river size*, though it is commonly assumed (Raymond et al., 2013; Linke et al., 2019; Liu et al., 2022; Andreadis et al., 2013; Allen & Pavelsky, 2018). We show empirically that river size is also fractal across spatial scales.

In basins where river width measurements are complete, such as our field survey of the South St. Vrain Creek Basin and other field surveys of headwater catchments (Allen et al., 2018), river size distributions are consistently described by a log-normal function. However, comprehensive surveys of river width are impractical at large spatial scales and statistical extrapolations must be employed to estimate the surface area of unmeasured rivers. The log-normal distribution of river widths at multiple spatial scales in the Mississippi River Basin has been demonstrated through field measurements (Moody & Troutman, 2002), but the scope of that study was limited to four individual reaches. Using stream order to integrate river widths measured in four nested

basins, we find that the statistical characteristics of the distribution of river widths are similar for rivers of all stream orders in the Mississippi River Basin. The consistent fit of a log-normal function to rivers of each stream order found in this study provides empirical evidence supporting the fractal nature of river size at all spatial scales.

The processes controlling river size at local, regional, and global scales are a pervasive research focus in fluvial geomorphology. Previous work has shown that discharge is a first order control on river width (Leopold & Maddock, 1953; Parker, 1978; Dunne and Jerolmack, 2020). Other researchers have presented a first order relationship between contributing drainage area and river width (Frasson et al., 2019). Both discharge and drainage area are closely correlated with Strahler stream order (r = 0.71 and 0.91, respectively) (Hughes et al., 2011). Given the relationships between river width and both discharge and drainage area, and the correlations between stream order and both discharge and drainage area, it follows that stream order is a predictor of river width; indeed, Hughes et al., 2011 also report a Spearman correlation coefficient of 0.73 between stream order and river width. Variability in discharge and drainage area, bed and bank sediment size, cohesion of bed and bank material, slope, critical shear stress and many other geomorphic parameters produce the log-normally distributed variability in width around a mean value, but the location parameter of the log-normal fit is associated with the range of discharge and drainage area characteristic of each stream order. The reason for the consistent log-normal fit of river size distributions across stream orders is currently unknown but is consistent with the distribution of river size found at other spatial scales (Moody & Troutman, 2002; Allen et al., 2018).

We acknowledge that stream order is an imperfect analogue for river size given its intended use as a system to describe position within branching river networks (Strahler, 1957), the dependency of map spatial resolution in assigning stream order (Scheidegger, 1966), and the temporal fluctuation of stream order as active drainage networks expand and contract (Godsey & Kirchner, 2014; Allen et al., 2018; Barefoot et al., 2019). However, we chose to use stream order in this analysis because of its rich history of use in fluvial geomorphology and to make this study comparable to others.

The fractal nature of river basins is obscured when only part of the river network is measured. Other researchers that measure river widths from remote sensing report a size distribution that departs from a log-normal function (Allen & Pavelsky, 2018). Our size distribution analysis at the basin scale also shows that the distributions of river widths measured from remote sensing in isolation are not consistently described by a log-normal function (see Table S1 and Fig. S2). This is due to both limitations inherent in remote sensing and finite size effects when measuring river widths at coarse spatial scales. At the lower tails of the river size distributions for each basin measured with remote sensing (see Fig. S2), there are rivers that are present on the landscape but missing from our analysis. Many small rivers are partially or completely obscured by vegetation and cannot be accurately detected from above. There is also a finite-size effect (Rodriguez-Iturbe & Rinaldo, 1997; Serafino et al., 2021) which causes size distributions to depart from known statistical distributions at their upper tails. The finite-size effect describes the breakdown of fractals in natural systems due to limitations of system size; in this case, there are not infinitely large rivers in the Mississippi River Basin so the upper tail of the measured distribution of river widths will trail off at its upper limit. Together, these factors may explain the departure from a consistent log-normal distribution when river widths measured from remote sensing are analyzed in isolation. However, our multi-scale analysis reveals a more realistic size distribution of rivers across spatial scales.

Our estimate for river surface area in the Mississippi River Basin (0.54% of land surface area) is consistent with previous estimates of the proportion of river surface area to land surface area globally (0.24% - 0.54%) (Raymond et al., 2013; Linke et al., 2019; Allen & Pavelsky, 2018; Downing et al., 2012; Liu et al., 2022), and within the Mississippi River Basin (0.33% - 0.78%) (Morgan, 2022; Raymond et al., 2013). However, most studies that estimate river surface area at large spatial scales do not adequately account for the surface area contribution of small headwater rivers. For example, the Pareto size distribution found by Allen & Pavelsky, 2018 for rivers ≥ 90

m wide is shown plotted on top of our synthetic width dataset in Fig. 5. This Pareto function has a lower bound of the median width of first order rivers reported by Allen et al., 2018 (0.32 m). This extrapolation represents an underestimate of the surface area of narrow rivers and does not include the smallest rivers (< 0.32 m wide) at all. It is particularly important to accurately account for the surface area of small rivers because they emit greenhouse gases like CO_2, CH_4, and N_2O at a disproportionate rate (Hotchkiss et al., 2015; Marzadri et al., 2021). This further illustrates the value of multi-scale approaches when using statistical methods to estimate river surface area at large scales.

5. Conclusion

In this multi-scale study incorporating a combination of remote sensing and fieldwork, we find empirical evidence supporting the fractal nature of river size across spatial scales. We measured the width of rivers of every stream order in the Mississippi River Basin and find log-normal size distributions for rivers of all stream orders. Using these log-normal size distributions, we estimate that the total river surface area in the Mississippi River Basin is 0.54% of total land surface area which is comparable to previous estimates of river surface area within the basin and globally. By combining remote sensing observations with field observations of river widths, we are able to more accurately represent the surface area of small rivers which are disproportionate emitters of greenhouse gases.

We acknowledge that river surface area is temporally dynamic. River networks expand and contract as a result of changing hydrologic conditions. Additionally, the wetting and drying processes associated with an active drainage network are important for the role of rivers in biogeochemical cycling. Future studies should investigate the temporal variability of river surface area at multiple spatial scales to further constrain the global greenhouse gas flux at the surfaces of rivers.

References

1. Allen, G. H., & Pavelsky, T. M. (2018a). Global extent of rivers and streams. *Science*, *361*(6402), 585–588. https://doi.org/10.1126/science.aat0636
2. Allen, G. H., & Pavelsky, T. M. (2018b). *Global River Widths from Landsat (GRWL) Database (V01.01)* [dataset]. Zenodo. https://doi.org/10.5281/zenodo.1297434
3. Allen, G. H., Pavelsky, T. M., Barefoot, E. A., Lamb, M. P., Butman, D., Tashie, A., & Gleason, C. J. (2018). Similarity of stream width distributions across headwater systems. *Nature Communications*, *9*(1). https://doi.org/10.1038/s41467-018-02991-w
4. Andreadis, K. M., Schumann, G. J.-P., & Pavelsky, T. (2013). A simple global river bankfull width and depth database. *Water Resources Research*, *49*(10), 7164–7168. https://doi.org/10.1002/wrcr.20440
5. Barefoot, E., Pavelsky, T. M., Allen, G. H., Zimmer, M. A., & McGlynn, B. L. (2019). Temporally Variable Stream Width and Surface Area Distributions in a Headwater Catchment. *Water Resources Research*, *55*(8), 7166–7181. https://doi.org/10.1029/2018WR023877
6. Benstead, J. P., & Leigh, D. S. (2012). An expanded role for river networks. *Nature Geoscience*, *5*(10), 678–679. https://doi.org/10.1038/ngeo1593
7. Bhatt, P., & Maclean, A. L. (2023). Comparison of high-resolution NAIP and unmanned aerial vehicle (UAV) imagery for natural vegetation communities classification using machine learning approaches. *GIScience & Remote Sensing*, *60*(1), 2177448. https://doi.org/10.1080/15481603.2023.2177448
8. Ciais, P., Sabine, C., Bala, G., Bopp, L., Brovkin, V., & House, J. I. (2014). Carbon and other biogeochemical cycles. In *Climate Change 2013: The Physical Science Basis. Contribution of Working Group I to the Fifth Assessment Report of the Intergovernmental Panel on Climate Change Change* (pp. 465–570). Cambridge University Press.
9. De Cicco, L. A., Lorenz, D., Hirsch, R. M., Watkins, W., & Johnson, M. (2022). *dataRetrieval: R packages for discovering and retrieving water data available from Federal hydrologic web services* (2.7.12) [R]. U.S. Geological Survey. https://doi.org/10.5066/P9X4L3GE
10. Dingman, S. L. (2007). Analytical derivation of at-a-station hydraulic–geometry relations. *Journal of Hydrology*, *334*(1), 17–27. https://doi.org/10.1016/j.jhydrol.2006.09.021
11. Downing, J. A., Cole, J. J., Duarte, C. M., Middelburg, J. J., Melack, J. M., Prairie, Y. T., Kortelainen, P., Striegl, R. G., McDowell, W. H., & Tranvik, L. J. (2012). Global abundance and size distribution of streams and rivers. *Inland Waters*, *2*(4), 229–236. https://doi.org/10.5268/IW-2.4.502
12. Dunne, K. B. J., & Jerolmack, D. J. (n.d.). What sets river width? *Science Advances*, *6*(41), eabc1505. https://doi.org/10.1126/sciadv.abc1505
13. Frasson, R. P. de M., Pavelsky, T. M., Fonstad, M. A., Durand, M. T., Allen, G. H., Schumann, G.,

Lion, C., Beighley, R. E., & Yang, X. (2019). Global Relationships Between River Width, Slope, Catchment Area, Meander Wavelength, Sinuosity, and Discharge. *Geophysical Research Letters*, *46*(6), 3252–3262. https://doi.org/10.1029/2019GL082027
14. Fritz, K. M., Hagenbuch, E., D'Amico, E., Reif, M., Wigington Jr., P. J., Leibowitz, S. G., Comeleo, R. L., Ebersole, J. L., & Nadeau, T.-L. (2013). Comparing the Extent and Permanence of Headwater Streams From Two Field Surveys to Values From Hydrographic Databases and Maps. *JAWRA Journal of the American Water Resources Association*, *49*(4), 867–882. https://doi.org/10.1111/jawr.12040
15. Fryirs, K. A., Ralph, T. J., Larkin, Z. T., Tooth, S., Humphries, M., McCarthy, T., Hesse, P. P., & Mosimanyana, E. (2018). A nested hierarchical perspective to enhance interpretations and communication in fluvial geomorphology for use in water resources management: Lessons from the Okavango Delta, Botswana. *The Geographical Journal*, *184*(2), 192–207. https://doi.org/10.1111/geoj.12250
16. Godsey, S. E., & Kirchner, J. W. (2014). Dynamic, discontinuous stream networks: Hydrologically driven variations in active drainage density, flowing channels and stream order. *Hydrological Processes*, *28*(23), 5791–5803. https://doi.org/10.1002/hyp.10310
17. Grison, F., Mota, A. de A., & Kobiyama, M. (2021). Testing the Leopold-Maddock and the Dingman hydraulic geometry hypotheses with detailed measurements in a small river. *Hydrological Sciences Journal*, *66*(8), 1372–1382. https://doi.org/10.1080/02626667.2021.1925285
18. Haygarth, P. M., Wood, F. L., Heathwaite, A. L., & Butler, P. J. (2005). Phosphorus dynamics observed through increasing scales in a nested headwater-to-river channel study. *Linking Landscape Sources of Phosphorus and Sediment to Ecological Impacts in Surface Waters*, *344*(1), 83–106. https://doi.org/10.1016/j.scitotenv.2005.02.007
19. Horton, R. E. (1945). Erosional development of streams and their drainage basins; hydrophysical approach to quantitative morphology. *GSA Bulletin*, *56*(3), 275–370. https://doi.org/10.1130/0016-7606(1945)56[275:EDOSAT]2.0.CO;2
20. Hotchkiss, E. R., Hall Jr, R. O., Sponseller, R. A., Butman, D., Klaminder, J., Laudon, H., Rosvall, M., & Karlsson, J. (2015). Sources of and processes controlling CO2 emissions change with the size of streams and rivers. *Nature Geoscience*, *8*(9), 696–699. https://doi.org/10.1038/ngeo2507
21. Hughes, R. M., Kaufmann, P. R., & Weber, M. H. (2011). National and regional comparisons between Strahler order and stream size. *Journal of the North American Benthological Society*, *30*(1), 103–121. https://doi.org/10.1899/09-174.1
22. Kirchner, J. W. (1993). Statistical inevitability of Horton's laws and the apparent randomness of stream channel networks. *Geology*, *21*(7), 591–594. https://doi.org/10.1130/0091-7613(1993)021<0591:SIOHSL>2.3.CO;2
23. La Barbera, P., & Rosso, R. (1989). On the fractal dimension of stream networks. *Water Resources Research*, *25*(4), 735–741. https://doi.org/10.1029/WR025i004p00735
24. Lauerwald, R., Allen, G. H., Deemer, B. R., Liu, S., Maavara, T., Raymond, P., Alcott, L., Bastviken, D., Hastie, A., Holgerson, M. A., Johnson, M. S., Lehner, B., Lin, P., Marzadri, A., Ran, L., Tian, H., Yang, X., Yao, Y., & Regnier, P. (2023). Inland Water Greenhouse Gas Budgets for RECCAP2: 2. Regionalization and Homogenization of Estimates. *Global Biogeochemical Cycles*, *37*(5), e2022GB007658. https://doi.org/10.1029/2022GB007658
25. Leopold, L. B., & Maddock Jr., T. (1953). *The hydraulic geometry of stream channels and some physiographic implications* (Report 252; Professional Paper, p. 64). USGS Publications Warehouse. https://doi.org/10.3133/pp252
26. Linke, S., Lehner, B., Ouellet Dallaire, C., Ariwi, J., Grill, G., Anand, M., Beames, P., Burchard-Levine, V., Maxwell, S., Moidu, H., Tan, F., & Thieme, M. (2019). Global hydro-environmental sub-basin and river reach characteristics at high spatial resolution. *Scientific Data*, *6*(1), 283. https://doi.org/10.1038/s41597-019-0300-6
27. Liss, P. S., & Slater, P. G. (1974). Flux of Gases across the Air-Sea Interface. *Nature*, *247*(5438), 181–184. https://doi.org/10.1038/247181a0
28. Liu, S., Kuhn, C., Amatulli, G., Aho, K., Butman, D. E., Allen, G. H., Lin, P., Pan, M., Yamazaki, D., Brinkerhoff, C., Gleason, C., Xia, X., & Raymond, P. A. (2022). The importance of hydrology in routing terrestrial carbon to the atmosphere via global streams and rivers. *Proceedings of the National Academy of Sciences*, *119*(11), e2106322119. https://doi.org/10.1073/pnas.2106322119
29. Mandelbrot, B. B., & Wheeler, J. A. (1983). The fractal geometry of nature. *American Journal of Physics*, *51*(3), 286.
30. Martinez, F., Manriquez, H., Ojeda, A., & Olea, G. (2022). Organization Patterns of Complex River Networks in Chile: A Fractal Morphology. *Mathematics*, *10*(11). https://doi.org/10.3390/math10111806
31. Marzadri, A., Amatulli, G., Tonina, D., Bellin, A., Shen, L. Q., Allen, G. H., & Raymond, P. A. (2021). Global riverine nitrous oxide emissions: The role of small streams and large rivers. *Science of The Total Environment*, *776*, 145148. https://doi.org/10.1016/j.scitotenv.2021.145148
32. McFeeters, S. K. (1996). The use of the Normalized Difference Water Index (NDWI) in the delineation of open water features. *International Journal of Remote Sensing*, *17*(7), 1425–1432. https://doi.org/10.1080/01431169608948714
33. McIntosh, A. R., Greig, H. S., Warburton, H. J., Tonkin, J. D., & Febria, C. M. (2024). Ecosystem-size relationships of river populations and

communities. *Trends in Ecology & Evolution*. https://doi.org/10.1016/j.tree.2024.01.010
34. McNamara, J. P., Kane, D. L., & Hinzman, L. D. (1998). An analysis of streamflow hydrology in the Kuparuk River Basin, Arctic Alaska: A nested watershed approach. *Journal of Hydrology*, *206*(1), 39–57. https://doi.org/10.1016/S0022-1694(98)00083-3
35. Meyer, J. L., & Wallace, J. B. (2001). *Lost linkages and lotic ecology: Rediscovering small streams.*
36. Moody, J. A., & Troutman, B. M. (2002). Characterization of the spatial variability of channel morphology. *Earth Surface Processes and Landforms*, *27*(12), 1251–1266. https://doi.org/10.1002/esp.403
37. Morgan, J. (2022). *Characterizing River Width Across Spatial Scales in the Mississippi River Basin* [Masters]. Texas A&M University.
38. Morisawa, M. E. (1962). Quantitative Geomorphology of Some Watersheds in the Appalachian Plateau. *GSA Bulletin*, *73*(9), 1025–1046. https://doi.org/10.1130/0016-7606(1962)73[1025:QGOSWI]2.0.CO;2
39. Nikora, V. I. (1991). Fractal structures of river plan forms. *Water Resources Research*, *27*(6), 1327–1333. https://doi.org/10.1029/91WR00095
40. Nikora, V. I. (1994). On self-similarity and self-affinity of drainage basins. *Water Resources Research*, *30*(1), 133–137. https://doi.org/10.1029/93WR02017
41. Nikora, V. I., & Sapozhnikov, V. B. (1993). River network fractal geometry and its computer simulation. *Water Resources Research*, *29*(10), 3569–3575. https://doi.org/10.1029/93WR00966
42. Otsu, N. (1979). A threshold selection method from gray level histograms. *IEEE Transactions on Systems, Man, and Cybernetics*, *9*, 62–66.
43. Raymond, P. A., Hartmann, J., Lauerwald, R., Sobek, S., McDonald, C., Hoover, M., Butman, D., Striegl, R., Mayorga, E., Humborg, C., Kortelainen, P., Dürr, H., Meybeck, M., Ciais, P., & Guth, P. (2013). Global carbon dioxide emissions from inland waters. *Nature*, *503*(7476), 355–359. https://doi.org/10.1038/nature12760
44. Richey, J. E., Melack, J. M., Aufdenkampe, A. K., Ballester, V. M., & Hess, L. L. (2002). Outgassing from Amazonian rivers and wetlands as a large tropical source of atmospheric CO2. *Nature*, *416*(6881), 617–620. https://doi.org/10.1038/416617a
45. Rodriguez-Iturbe, I., & Rinaldo, A. (1997). *Fractal river basins: Chance and self-organization*. Cambridge University Press.
46. Rosentreter, J. A., Borges, A. V., Deemer, B. R., Holgerson, M. A., Liu, S., Song, C., Melack, J., Raymond, P. A., Duarte, C. M., Allen, G. H., Olefeldt, D., Poulter, B., Battin, T. I., & Eyre, B. D. (2021). Half of global methane emissions come from highly variable aquatic ecosystem sources. *Nature Geoscience*, *14*(4), 225–230. https://doi.org/10.1038/s41561-021-00715-2
47. Scheidegger, A. E. (1966). Statistical description of river networks. *Water Resources Research*, *2*(4), 785–790. https://doi.org/10.1029/WR002i004p00785
48. Serafino, M., Cimini, G., Maritan, A., Rinaldo, A., Suweis, S., Banavar, J. R., & Caldarelli, G. (2021). True scale-free networks hidden by finite size effects. *Proceedings of the National Academy of Sciences*, *118*(2), e2013825118. https://doi.org/10.1073/pnas.2013825118
49. Strahler, A. N. (1952). Dynamic basis of geomorphology. *GSA Bulletin*, *63*(9), 923–938. https://doi.org/10.1130/0016-7606(1952)63[923:DBOG]2.0.CO;2
50. Strahler, A. N. (1957). Quantitative analysis of watershed geomorphology. *Eos, Transactions American Geophysical Union*, *38*(6), 913–920. https://doi.org/10.1029/TR038i006p00913
51. Pavelsky, T.M., & Smith, L.C. (2008). RivWidth: A Software Tool for the Calculation of River Widths From Remotely Sensed Imagery. *IEEE Geoscience and Remote Sensing Letters*, *5*(1), 70–73. https://doi.org/10.1109/LGRS.2007.908305
52. Tarboton, D. G., Bras, R. L., & Rodriguez-Iturbe, I. (1988). The fractal nature of river networks. *Water Resources Research*, *24*(8), 1317–1322. https://doi.org/10.1029/WR024i008p01317
53. Venables, B., & Ripley, B. (2002). Modern Applied Statistics With S. In *Springer*. https://doi.org/10.1007/b97626
54. Wolf, A. F. (2012). *Using WorldView-2 Vis-NIR multispectral imagery to support land mapping and feature extraction using normalized difference index ratios*. *8390*, 83900N. https://doi.org/10.1117/12.917717

Supporting Information for

QUANTIFYING THE SIZE DISTRIBUTION OF RIVERS ACROSS SPATIAL SCALES

C.A. Boyd[1] and G.H Allen[1]

[1]Department of Geosciences, Virginia Tech, Blacksburg, VA

Contents of this file

Supplementary Methods

Figures S1 to S3

Tables S1 to S3

1. Supplementary Methods

To investigate the size distributions of rivers at different spatial scales, we use a nested basin approach. We use a combination of remote sensing imagery and field surveying to measure river width at increasingly smaller spatial scales within a continental scale basin. We then use these width measurements to describe the size distribution of rivers across spatial scales and make an estimate of river surface area. This statistical approach avoids a tedious width inventory of rivers that are not observable using remote sensing imagery and allows for more robust estimates of river surface area by accounting for the variability of statistical distributions of river size across spatial scales.

1.1 Study Areas

Our study areas consist of four drainage basins in the interior of the North American continent: the Mississippi River Basin draining 3.3 million km^2, the Platte River Basin draining 220,000 km^2, the St. Vrain Creek Basin draining 2,500 km^2, and the South St. Vrain Creek Basin draining 14 km^2. These study areas were chosen for their size, ability to be viewed from above with minimal obscuring vegetation, and convenience for fieldwork.

We use river width measurements from remote sensing at larger spatial scales where rivers are easily observable from above: in the Mississippi River Basin, we use the Global River Widths from Landsat (GRWL) product (Allen & Pavelsky, 2018) which is based on Landsat 30 m resolution multispectral satellite imagery; in the Platte River Basin, we use Sentinel-2 10 m resolution multispectral satellite imagery; in the St. Vrain Creek Basin, we use National Agriculture Imagery Program (NAIP) 1 m resolution multispectral aerial imagery. In the South St. Vrain Creek Basin, we conducted a field survey of river widths.

1.2 Image Acquisition and Preprocessing

Our goal when selecting remotely sensed imagery was to match the time of year between image sources. For this study, the limiting factor for selecting the timing of the imagery was the availability of NAIP imagery which is generally available in the "leaf-on" period (July-August in the St. Vrain Creek Basin). River width measurements over the Mississippi River Basin from GRWL were taken at mean annual discharge. When selecting Sentinel-2 imagery, we visually compared mosaics of the least cloudy images during this time period for different years and found that the mosaic from July-September 2019 had the most continuous river network in the Platte River Basin. When selecting NAIP imagery, we used a similar approach and found that the mosaic from July-August 2021 had the most continuous river network in the St. Vrain Creek Basin. We selected the timing of field surveys of the South St. Vrain Creek Basin to match this time period, July 6, 2023 – August 6, 2023.

All imagery was acquired through the Google Earth Engine (GEE) catalog and processed in GEE before exporting to Google Drive for further processing and analysis. We first filtered the image collection from each data source to the dates of interest. We also filtered the image collection from each data source to a polygon of the basin boundary with a 500 m buffer. We sorted the remaining Sentinel-2 images from least to most cloudy using the 'CLOUDY_PIXEL_PERCENTAGE' attribute and

masked any remaining clouds using a bit mask function. NAIP imagery is made available with very little cloud cover, so we did not process this imagery for clouds. NAIP flyover images were mosaicked to cover the buffered study area. Rectangle polygon slivers that extend from the top to the bottom of a mosaic image were created in GEE based on the width of the bounding box of the buffered study area and the number of rectangle slivers desired to enable export at the highest possible spatial resolution. The number of rectangles used to export each image was determined through trial and error with the goal of minimizing the number of rectangles while allowing for efficient processing and export from GEE.

1.3 Water Detection Algorithm

For each rectangle sliver, we created a near infrared (NIR) and normalized difference water index (NDWI) image in GEE. NDWI is a ratio of the green and NIR bands (blue and NIR for NAIP (Bhatt & Maclean, 2023; Wolf, 2012)) that can be used to indicate the presence of water (McFeeters, 1996). We used the Otsu image segmentation method (Otsu, 1979) to determine an optimized NIR and NDWI threshold to differentiate between "water" and "not water" classes for each scene. We used existing centerlines from NHDPlus V2 to create a buffer around rivers in each image that covered a roughly equal proportion of "water" and "not water" pixels. Platte River initial centerlines were filtered to only include rivers of order ≥ 8. Within each rectangle sliver, the river widths reported in the GRWL database (excluding widths reported over reservoirs) were averaged to determine the average width of rivers in the buffer region. This value was divided by the pixel spatial resolution (10 m) to determine a buffer width around the NHDPlus V2 centerlines within each rectangle sliver. St. Vrain Creek initial centerlines were filtered to only include rivers of order ≥ 5. Widths reported in the GRWL dataset within the St. Vrain Creek basin are insufficient to estimate average river width in the NAIP scenes; therefore, width was estimated using a relationship between width and stream order reported by Downing et al., 2012 for each polyline segment in the initial centerline shapefile (Downing et al., 2012):

$$w = 0.542e^{0.824\omega} \quad (6)$$

Within each rectangle sliver, the estimated river widths along the initial centerlines were averaged to estimate the average width of rivers in the region of interest. This value was divided by the pixel spatial resolution (1 m) to determine a buffer width around the NHDPlus V2 centerlines within each rectangle sliver. Histograms of NIR and NDWI values within each buffer region were analyzed in GEE to identify scene-specific thresholds that maximized the inter-class variance. We used these thresholds to create a water mask within each scene where pixels that have a NIR value less than the calculated NIR threshold and a NDWI value greater than the calculated NDWI threshold are masked as water pixels. The water masks, NDWI images, and true color images were exported from GEE to Google Drive in 8-bit GEOTIFF format for further processing and analysis.

1.4 Water Mask Cleaning

All rectangle slivers constituting a single UTM zone were stitched together in ESRI ArcGIS Pro using the "Mosaic to New Raster" tool and exported as 8-bit GEOTIFF files. The St. Vrain Creek Basin does not span multiple UTM zones, so it was treated as a single scene. Visual obstructions of the channel as viewed from above create discontinuities and artificial contractions of the river network in the water masks. Additionally, misclassified roads as well as shaded and built-up areas create artificial expansions of the river network in the water masks. To prepare the water masks for the RivSelect and RivWidth routines (Pavelsky & Smith, 2008), these discontinuities and artificial contractions/expansions were corrected by manually editing pixel values in Adobe Photoshop (Allen & Pavelsky, 2018). The water mask .tif files were overlain on true color and NDWI reference images. The water masks were converted to RGB and the "paint bucket" tool was used to give all water pixels a red value of 255. Reservoirs in the river network were identified manually and water pixels covering reservoirs were given a red value of 127. Canals in the river network were identified manually and water pixels covering canals were given a red value of 64. The "brush" tool was used to manually edit pixel values in the water masks to correct for discontinuities and artificial contractions/expansions in the river network.

Much of this work was done by two undergraduate research assistants, each checking each other's work for a more consistent product. After the water mask was cleaned and labeled, a color version of the water mask was saved. Another grayscale water mask without reservoirs and canals labeled was saved for subsequent RivSelect analysis.

1.5 RivSelect and RivWidth

RivSelect is an IDL script that masks all water pixels in the cleaned water mask that are not connected to the river network, producing an ENVI formatted .img channel mask with only the continuous river network classified (Pavelsky & Smith, 2008). RivSelect was used iteratively when cleaning and checking the water mask in Photoshop to find discontinuities in the river network by comparing the water mask and the channel mask produced by RivSelect.

The final channel mask produced by RivSelect was input to the RivWidth IDL script (Pavelsky & Smith, 2008). RivWidth identifies river centerlines and calculates the river width orthogonal to the centerlines based on the pixel width of the channel mask. RivWidth produces a polyline shapefile of the river centerlines with width information as an attribute for each line segment, and a raster product that is identical to the channel mask produced by RivSelect. To label the reservoirs and canals in each scene, the centerline shapefiles were overlain on the color water mask .tif files in ArcGIS Pro. The pixel value of the color water mask under each centerline segment was extracted using the "Zonal Statistics as Table" tool and then joined to the attribute tables of the centerline shapefiles. New fields were created in the centerline attribute tables for tagging both reservoirs and canals. If the pixel value of the color water mask for a given centerline segment was 255, that segment was given a value of 0 in both label fields. If the pixel value of the color water mask was 127, that segment was given a value of 1 in the reservoir label field and a value of 0 in the canal label field. If the pixel value of the color water mask was 64, that segment was given a value of 0 in the reservoir label field and a value of 1 in the canal label field. To label the raster product, all pixels with a red value of 127 (reservoir pixels) and 64 (canal pixels) in the color water mask were copied and pasted into the RivWidth raster product in Adobe Photoshop.

1.6 Validation of Remotely Measured Widths

River width measurements from remote sensing imagery were validated by comparing measurements to USGS reported widths at gaging stations. In each study area, all USGS reported paired width and discharge measurements at gaging stations located on rivers that we measured were identified and downloaded using the dataRetrieval package (De Cicco et al., 2022) in R. At each gaging station, mean annual discharge was calculated using daily discharge values from all years with complete records and used to filter paired width and discharge measurements to only include paired measurements within 10% of mean annual discharge. The mean of the remaining USGS reported width measurements at each gage was compared to the mean of the 10 closest remotely sensed river widths.

1.7 NAIP Width Correction

The availability of NAIP imagery during the leaf-on period does not correspond to the time of year when rivers in the St. Vrain Creek Basin are typically at mean annual discharge. Therefore, we corrected NAIP measured widths using a regional rating curve approach. All paired width and discharge measurements at each USGS gaging station in the St. Vrain Creek Basin were accessed using the dataRetrieval package (De Cicco et al., 2022) in R. Discharge measurements were converted to percentile discharge using the entire record of daily discharge measurements for complete years at each gage. We then used a non-linear least squares regression to fit exponential functions relating width and percentile discharge at each gage. We used a mean of each exponential function parameter for all gages in the St. Vrain Creek Basin to create a regional rating curve relating width and percentile discharge. We then found the mean percentile discharge during the Sentinel-2, NAIP, and fieldwork period of observation (July – September 2019, July – August 2021, and July 6 – August 6, 2023, respectively). Using the regional rating curve, we calculated the percentage change in width between the mean percentile discharge during the NAIP observation period and the mean of the mean percentile discharges during the Sentinel-2 and

fieldwork observation periods. This percentage change in width (25%) was used as a multiplicative scaling factor to correct NAIP measured widths.

1.8 Field Surveying

The width and length of all rivers in a headwater catchment of the South St. Vrain Creek were surveyed between July 6 – August 6, 2023. We define a river here as water flowing in a channel. Widths were measured using a tape measure or laser range finder every 10 m while pacing the length of every river. Paces were remeasured regularly throughout the field campaign. The river network was divided into segments with a new segment beginning at every confluence or major river crossing. The Strahler stream order for each segment was assigned manually. Rivers were mapped in Google Earth Pro using handheld GPS tracks and length measurements. We quantified measurement error using repeat width surveys of 100 m long river reaches throughout the duration of the field campaign. We surveyed each segment five times within one hour and compared width measurements to find a mean standard error of 1 cm.

1.9 Stream Order Data Fusion

To assign Strahler stream order to the remotely sensed river width measurements, we performed a spatial join of the river centerlines and flowlines from NHDPlus V2 in ArcGIS Pro. According to NHDPlus V2, the mainstem of the South St. Vrain Creek at our field site was order 1; however, we measured this segment as order 5. When the South St. Vrain Creek network was surveyed, intermittent segments (order 0) were flowing; therefore, we assume that the mainstem of the South St. Vrain Creek is typically order 4. We increased stream order from NHDPlus V2 by three to match the assumed order of rivers measured in the field. The measured order of river segments in the South St. Vrain Creek were maintained to reflect the hydrologic conditions of when they were surveyed.

1.10 Distribution Fitting

Statistical distributions were fitted to river width measurements (with canals and reservoirs removed) using maximum likelihood estimation in R. To ensure consistency across datasets, width measurements were sampled to 30 m measurement spacing to match GRWL. To improve measurement accuracy in the stream order size distribution analysis, river width measurements in each dataset were restricted by stream order: GRWL measurements ≥ order 11, Sentinel-2 measurements ≥ order 8, NAIP measurements ≥ order 5, and all field measurements. We attempted to fit log-normal, Pareto, gamma, and Weibull statistical distributions (Equations 2-5) to the width data and assessed goodness of fit and optimized the fit parameters using a single sample, two-tailed Kolmogorov-Smirnov test (Venables & Ripley, 2002).

1.11 Surface Area Estimation

We estimated the total length of rivers of each stream order in the Mississippi River Basin using river length and number from NHDPlus V2 and Horton scaling principles (Horton, 1945) (see Fig. S1). We fit statistical distributions to our width measurements of rivers of each order and estimated the parameters of those fits using maximum likelihood estimation. We then created a synthetic dataset of width measurements for rivers of each order with a measurement spacing of 30 m using the total length of rivers of each order. Finally, we multiplied each width measurement by the length between measurements (30 m) and summed to get an estimate of total river surface area in the Mississippi River Basin.

$$n_\omega = a \times b^\omega$$

$$\bar{l}_\omega = c \times d^\omega$$

$$R_n = \frac{n_\omega}{n_{\omega+1}}$$

$$R_l = \frac{\bar{l}_{\omega+1}}{\bar{l}_\omega}$$

$$a = \frac{n_\omega}{R_n^{-\omega}}$$

$$c = \frac{\bar{l}_\omega}{R_l^\omega}$$

$\omega = stream\ order$
$n_\omega = number\ of\ rivers\ of\ order\ \omega$
$\bar{l}_\omega = average\ length\ of\ rivers\ of\ order\ \omega$
$a, b, c, d = fitted\ constants$
$R_n = bifurcation\ ratio, ratio\ of\ the\ number\ of\ rivers\ of\ order\ \omega\ and\ \omega + 1$
$R_l = length\ ratio, ratio\ of\ the\ average\ length\ of\ rivers\ of\ order\ \omega + 1\ and\ \omega$

Figure S1. Horton scaling ratios (Horton, 1945) used to determine the total length of rivers of each order in the Mississippi River Basin.

Table S1. Log-normal, Pareto, gamma, and Weibull probability density function parameters fit to river width measurements in each basin and Wasserstein distance and Kolmogorov-Smirnov goodness of fit test results.

Basin	South St. Vrain Creek	St. Vrain Creek	Platte River	Mississippi River
N Observations	1148	14506	126060	1384979
Log-normal Distribution				
Location, μ	-0.336	1.915	3.884	4.671
Scale, σ	1.055	0.748	1.010	0.977
Wasserstein Distance	0.211	0.889	6.950	31.872
K-S D	0.046	0.084	0.097	0.115
K-S p	0.015	0.000	0.000	0.000
Pareto Distribution				
Scale, x_m	0.305	6.247	14	42
Shape, α	0.800	1.520	0.621	0.820
Wasserstein Distance	32.873	8.971	57111.03	33149.38
K-S D	0.139	0.174	0.212	0.097
K-S p	0.000	0.000	0.000	0.000
Gamma Distribution				
Shape, α	0.937	2.128	1.109	1.049
Rate, β	0.705	0.244	0.014	0.006
Wasserstein Distance	0.380	0.385	14.102	50.832
K-S D	0.134	0.054	0.095	0.164
K-S p	0.000	0.000	0.000	0.000
Weibull Distribution				
Shape, γ	0.887	1.494	0.998	0.941
Scale, α	1.235	9.725	81.174	178.49
Wasserstein Distance	0.273	0.526	11.914	43.838
K-S D	0.112	0.056	0.114	0.167
K-S p	0.000	0.000	0.000	0.000

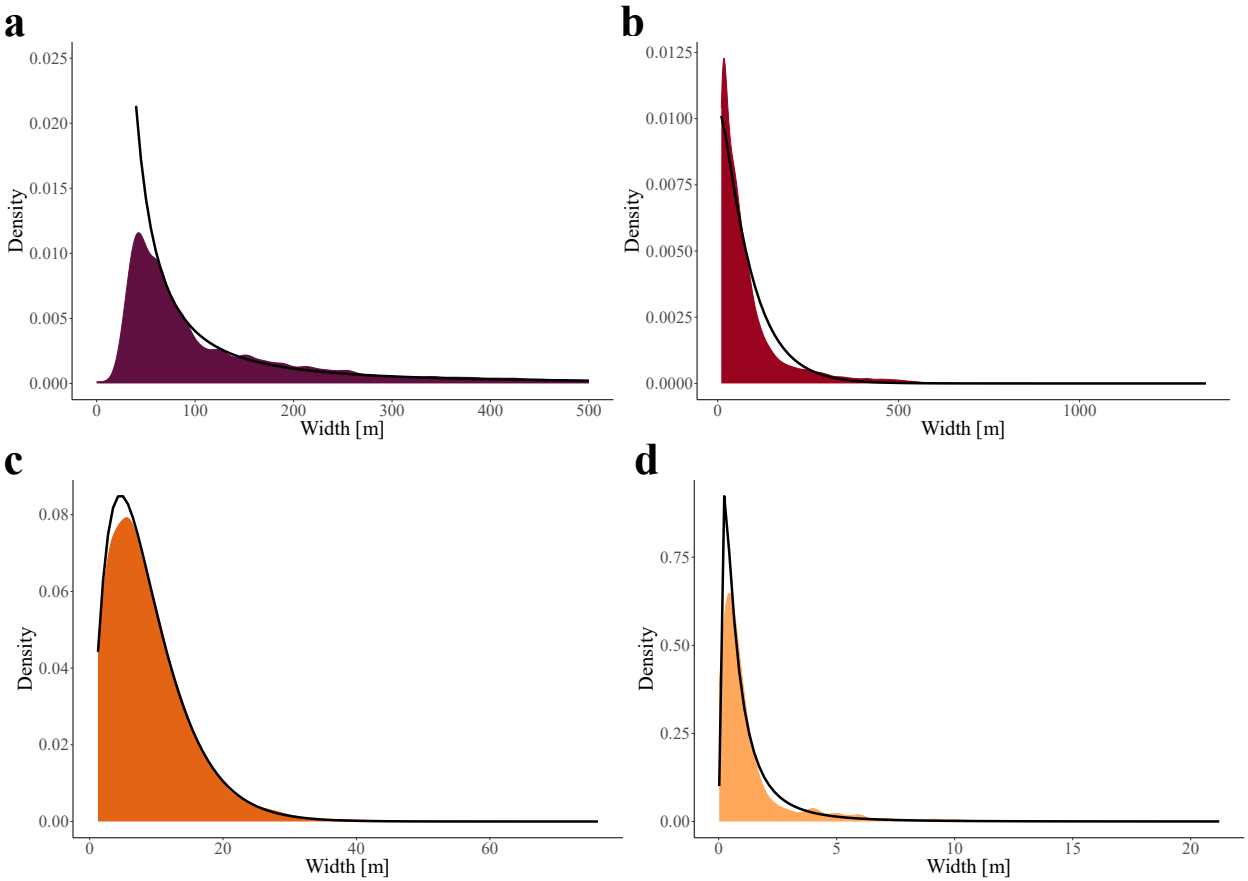

Figure S2. Density plots of river widths measured using each data source. a) Density plot of river widths in the Mississippi River Basin from GRWL with a fitted Pareto probability density function; b) Density plot of river width measurements in the Platte River Basin from Sentinel-2 with a fitted gamma probability density function; c) Density plot of river width measurements in the St. Vrain Creek Basin from NAIP with a fitted gamma probability density function; d) Density plot of river width measurements in the South St. Vrain Creek Basin from fieldwork with a fitted log-normal probability density function.

Table S2. Log-normal, Pareto, gamma, and Weibull probability density function parameters fit to river width measurements of each stream order and Wasserstein distance and Kolmogorov-Smirnov goodness of fit test results.

Stream Order	1	2	3	4	5	6	7	8	9	10	11	12	13
N Observations	488	318	220	67	2869	5954	3232	21017	26965	34396	165303	70434	52952
Log-normal Distribution													
Location, μ	-0.961	-0.415	0.202	1.085	1.628	1.830	2.386	3.691	3.749	3.904	5.813	6.003	6.744
Scale, σ	0.784	0.736	0.740	0.759	0.512	0.715	0.426	0.972	0.981	0.596	0.724	0.563	0.494
Wasserstein Distance	0.068	0.095	0.192	0.950	0.660	0.984	0.684	12.783	12.075	4.312	27.531	27.188	106.887
K-S D	0.043	0.042	0.039	0.077	0.182	0.093	0.105	0.142	0.116	0.106	0.043	0.072	0.112
K-S p	0.329	0.638	0.896	0.796	0.000	0.000	0.000	0.000	0.000	0.000	0.000	0.000	0.000
Pareto Distribution													
Scale, x_m	0.229	0.406	1.524	4.001	6.247	2.499	9.995	14.000	14.000	50.000	150.000	256.000	618.000
Shape, α	1.140	1.207	1.943	1.604	2.985	0.838	2.655	0.654	0.657	2.231	1.024	1.517	2.285
Wasserstein Distance	0.473	0.297	0.244	1.879	1.128	351.275	1.776	84722.726	10102.493	15.279	1042.550	238.812	170.089
K-S D	0.141	0.179	0.058	0.216	0.314	0.256	0.132	0.206	0.170	0.148	0.198	0.140	0.123
K-S p	0.000	0.000	0.826	0.056	0.000	0.000	0.000	0.000	0.000	0.000	0.000	0.000	0.000
Gamma Distribution													
Shape, α	1.534	1.887	1.958	1.765	4.498	2.385	5.907	1.287	1.235	3.285	2.302	3.402	6.283
Rate, β	2.800	2.144	1.213	0.438	0.787	0.306	0.498	0.021	0.018	0.056	0.005	0.007	0.007
Wasserstein Distance	0.118	0.150	0.191	0.758	0.424	0.409	0.754	7.230	7.750	1.624	22.979	48.386	35.594
K-S D	0.110	0.076	0.085	0.135	0.152	0.075	0.089	0.132	0.136	0.068	0.050	0.092	0.069
K-S p	0.000	0.052	0.082	0.158	0.000	0.000	0.000	0.000	0.000	0.000	0.000	0.000	0.000
Weibull Distribution													
Shape, γ	1.096	1.264	1.344	1.246	2.287	1.663	2.261	1.134	1.093	1.861	1.518	1.774	2.669
Scale, α	0.572	0.958	1.776	4.373	6.440	8.753	13.364	65.142	69.569	65.636	471.630	534.467	1031.858
Wasserstein Distance	0.149	0.148	0.242	0.609	0.398	0.366	1.422	6.875	6.904	3.094	34.614	57.786	64.588
K-S D	0.133	0.091	0.099	0.140	0.126	0.066	0.125	0.121	0.126	0.067	0.069	0.131	0.096
K-S p	0.000	0.010	0.027	0.133	0.000	0.000	0.000	0.000	0.000	0.000	0.000	0.000	0.000

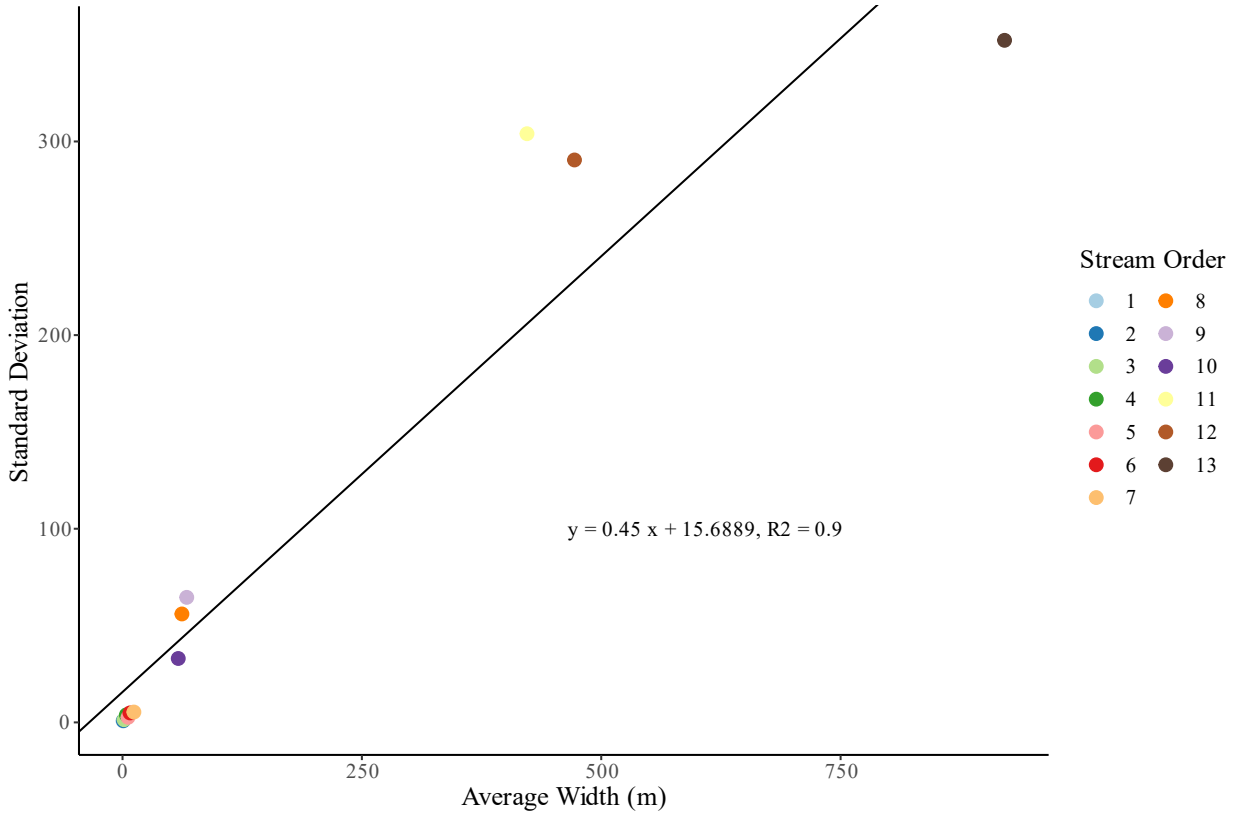

Figure S3. Linear regression between average width and standard deviation of width by stream order.

Table S3. River lengths calculated using Horton scaling principles (Horton, 1945; Downing et al., 2012) (see Fig. S1).

Order	Number	Avg Length [km]	Total Length [km]
1	16,777,216	0.128	2,141,667.385
2	4,194,304	0.284	1,191,237.511
3	1,048,576	0.632	662,589.727
4	262,144	1.406	368,545.435
5	65,536	3.128	204,992.218
6	16,384	6.959	114,020.702
7	4,096	15.483	63,420.557
8	1,024	34.449	35,275.761
9	256	76.645	19,621.072
10	64	170.525	10,913.626
11	16	379.398	6,070.373
12	4	844.115	3,376.461
13	1	1,878.054	1,878.054